# Torsion of Rectangular HSS and Box Section Members: A Critical Review

BO DOWSWELL

## ABSTRACT

The purposes of this paper are to summarize the research on the torsional performance of square and rectangular hollow section members and compare the available experimental results to the applicable provisions in the AISC *Specification* (2022). A review of the research on the torsional strength of square and rectangular hollow section members revealed 49 experimental tests from 11 projects. A first-order reliability analysis was used to calculate appropriate resistance factors for the current design equations, revealing inconsistent reliability indices that are dependent on the predicted failure mode. Revisions are proposed for the provisions in AISC *Specification* Section H3.1 that result in a simpler design method with increased accuracy. Also, the accuracy of serviceability rotation calculations is evaluated using the available experimental data.

**Keywords:** torsion, rectangular HSS, box section, serviceability rotation.

## INTRODUCTION

Square and rectangular hollow sections are often used to resist twisting because they are more efficient at resisting torsional loads than open sections. These hollow sections are defined as HSS or box sections based on the manufacturing and fabrication methods. The AISC *Specification* (2022) Glossary defines two types of hollow sections:

- Box section: Square or rectangular doubly symmetric members made with four plates welded together at the corners such that it behaves as a single member.
- HSS (hollow structural section): Square, rectangular or round hollow structural steel section produced in accordance with one of the product specifications in Section A3.1a(b).

The torsional strength of square and rectangular HSS shapes is evaluated according to AISC *Specification* Section H3.1. Both the yielding and wall buckling limit states are addressed only for HSS shapes. The design method is based on the classical plate buckling equation and research related primarily to I-shaped member webs subjected to shear. Although the load transfer mechanism is similar to that of I-shaped beam webs, the accuracy of these equations has not been established for HSS members subjected to torsion.

Bo Dowswell, PhD, PE, Principal, ARC International, LLC, Birmingham, Ala.
Email: bo@arcstructural.com

Paper No. 2024–09R

The purposes of this paper are to summarize the research on the torsional performance of square and rectangular hollow section members and compare the available experimental results to the applicable provisions in the AISC *Specification*. A first-order reliability analysis is used to calculate appropriate resistance factors for the current design equations and revisions to the AISC *Specification* are proposed. Also, the accuracy of serviceability rotation calculations is evaluated using the available experimental data.

## AISC *SPECIFICATION* SECTION H3

The nominal torsional strength of an HSS member is calculated with Equation H3-1 in AISC *Specification* Section H3.1.

$$T_n = F_{cr}C \qquad \text{(AISC } Spec. \text{ H3-1)}$$

For rectangular HSS members, the critical shear stress is determined as follows.

When $\frac{h}{t} \le 2.45\sqrt{\frac{E}{F_y}}$

$$F_{cr} = 0.6F_y \qquad \text{(AISC } Spec. \text{ H3-3)}$$

When $2.45\sqrt{\frac{E}{F_y}} < \frac{h}{t} \le 3.07\sqrt{\frac{E}{F_y}}$

$$F_{cr} = 0.6F_y \frac{2.45\sqrt{\frac{E}{F_y}}}{\left(\frac{h}{t}\right)} \qquad \text{(AISC } Spec. \text{ H3-4)}$$

When $3.07\sqrt{\frac{E}{F_y}} < \frac{h}{t} \le 260$

$$F_{cr} = \frac{0.458\pi^2 E}{\left(\frac{h}{t}\right)^2} \quad \text{(AISC } \textit{Spec.}\text{ H3-5)}$$

where

$C$ = torsional modulus constant, in.$^3$
$E$ = modulus of elasticity, ksi
$F_y$ = specified minimum yield stress, ksi
$h$ = flat width of longer side, in.
$t$ = design wall thickness, in.
$\phi_T$ = 0.90 (LRFD)
$\Omega_T$ = 1.67 (ASD)

The cross-sectional dimensions of a rectangular HSS are shown in Figure 1.

## AISC *SPECIFICATION* SECTION G2

For rectangular HSS members, torques are resisted primarily by shear in the walls. Because the behavior of HSS walls is similar to that of I-shaped member webs subjected to shear loads, AISC *Specification* Section G2.1 is reviewed in this section of the paper. The nominal shear strength of I-shaped members is calculated with Equation G2-1 in AISC *Specification* Section G2.1.

$$V_n = 0.6F_y A_w C_{v1} \quad \text{(AISC } \textit{Spec.}\text{ G2-1)}$$

where $A_w$ is the web area. Built-up members are addressed in Section G2.1(b), where the web strength coefficient, $C_{v1}$, is defined as follows.

When $\frac{h}{t} \le 1.10\sqrt{\frac{k_v E}{F_y}}$

$$C_{v1} = 1.0 \quad \text{(AISC } \textit{Spec.}\text{ G2-3)}$$

When $\frac{h}{t} > 1.10\sqrt{\frac{k_v E}{F_y}}$

$$C_{v1} = \frac{1.10\sqrt{\frac{k_v E}{F_y}}}{\left(\frac{h}{t}\right)} \quad \text{(AISC } \textit{Spec.}\text{ G2-4)}$$

According to Section G2.1(b)(2)(i), $k_v = 5.34$ for webs without transverse stiffeners.

## EUROCODE 3, PART 1-1

Eurocode 3, Part 1-1 (CEN, 2005) Section 6.2.7(7) states, "As a simplification, in the case of a member with a closed hollow cross-section, such as a structural hollow section, it may be assumed that the effects of torsional warping can be neglected." The design philosophy for closed hollow sections in Part 1-1 Section 6.2.7(8) is similar to that of AISC *Specification* Section H3.1, with the shear strength calculated using the provisions for plated structural elements in Eurocode 3, Part 1-5 (CEN, 2006).

Part 1-5 Section 5 specifies the design method for the shear resistance of plate elements. The factor $\eta$ is used to estimate the ultimate shear buckling strength. Here, $\eta = 1.2$ is recommended for calculating the shear strength of steel grades up to and including S460 ($F_y$ = 460 MPa = 67 ksi), and $\eta = 1.0$ is recommended for higher strength steels. For values of $\eta$ greater than 1.0, the increased strength is attributed to strain hardening (Beg et al., 2010). Because large inelastic rotations may be required to obtain the torsional strengths calculated with $\eta > 1.0$, $\eta = 1.0$ is used in the equations below. This limits the critical stress to the shear yield stress. Where applicable, the variable name symbols defined in the AISC *Specification* were used in lieu of the Eurocode symbols. This is intended to make direct comparisons between the two design requirements easier.

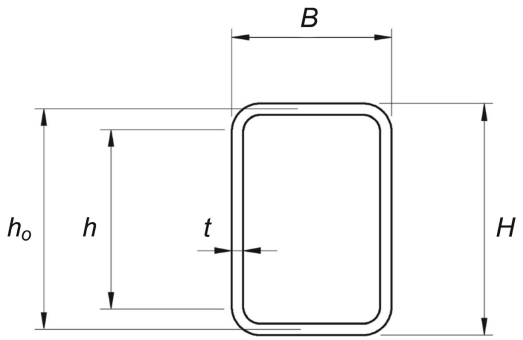


*Fig. 1. Cross-sectional dimensions of a rectangular HSS.*

The critical shear stress is

$$F_{cr} = \frac{F_y C_v}{\sqrt{3}} \tag{1}$$

When $\lambda_T < 0.83$

$$C_v = 1.00 \tag{2}$$

When $\lambda_T \geq 0.83$

$$C_v = \frac{0.83}{\lambda_T} \tag{3}$$

The slenderness is

$$\lambda_T = \sqrt{\frac{\tau_y}{\tau_e}} = 0.76\sqrt{\frac{F_y}{\tau_e}} \tag{4}$$

where the shear yield stress, $\tau_y$, is $F_y/\sqrt{3}$. The elastic critical shear stress, $\tau_e$, of an infinitely long plate with simply supported edges subjected to shear is (Ziemian, 2010)

$$\tau_e = k_v \frac{\pi^2 E}{12(1-\nu^2)\left(\frac{h}{t}\right)^2} \tag{5}$$

where

$k_v$ = buckling coefficient
= 5.34 for plates with simply supported edges
= 8.98 for plates with clamped edges
$\nu$ = Poisson's ratio

When the elements are assumed to be simply supported, the slenderness can be determined by substituting Equation 5 into Equation 4 with $k_v = 5.34$.

$$\lambda_T = 0.35\frac{h}{t}\sqrt{\frac{F_y}{E}} \tag{6}$$

For comparison, the Eurocode provisions can be written in the same format as the AISC *Specification*. To make the comparisons easier, the shear yield stress, $\tau_y = 0.6F_y$, is used in lieu of $\tau_y = F_y/\sqrt{3}$.

When $\frac{h}{t} < 2.4\sqrt{\frac{E}{F_y}}$

$$F_{cr} = 0.6F_y \tag{7}$$

When $\frac{h}{t} \geq 2.4\sqrt{\frac{E}{F_y}}$

$$F_{cr} = 0.6F_y \frac{2.4\sqrt{\frac{E}{F_y}}}{\left(\frac{h}{t}\right)} \tag{8}$$

## SECTION PROPERTIES

The torsional modulus constant, $C$, is used in strength calculations, and the torsional inertia constant, $J$, is used in rotational stiffness calculations. As discussed in AISC *Specification* Section H3.1 Commentary, the torsional modulus constant can be defined using a membrane analogy. The area enclosed by the sectional mid-thickness is

$$A_o = (B-t)(H-t) - r_m^2(4-\pi) \tag{9}$$

The torsional modulus constant is

$$C = 2tA_o = 2t\left[(B-t)(H-t) - r_m^2(4-\pi)\right] \tag{10}$$

where

$B$ = overall width, in.
$H$ = overall height, in.
$r_m$ = mid-thickness corner radius, in.

Assuming $r_m = 1.5t$, which is based on an outside corner radius, $r_o$, of $2t$, results in the HSS torsional constant in the User Note in AISC *Specification* Section H3.1:

$$C = 2t(B-t)(H-t) - 4.50t^3(4-\pi) = 2t(B-t)(H-t) - 3.86t^3 \tag{11}$$

For the rectangular HSS materials listed in *Specification* Section A3.1a.(b) [ASTM A500 (2021), A501 (2014), A1085 (2015a), and A618 (2015b)], the maximum permissible outside corner radius is $3t$. Equation 12, which is based on $r_m = 2.5t$, can be used for this condition.

$$C = 2t(B-t)(H-t) - 12.5t^3(4-\pi) = 2t(B-t)(H-t) - 10.7t^3 \tag{12}$$

The torsional inertia constant is

$$J = \frac{4tA_o^2}{p_m} \tag{13}$$

The mid-thickness perimeter is

$$p_m = 2(B+H-4r_o) + 2\pi r_m = 2\left[B+H-2t+r_m(\pi-4)\right] \tag{14}$$

where

$r_o$ = outside corner radius, in.

Equations 10 through 13 were derived using thin-wall theory, which is based on the assumption that the shear stress is constant across the wall thickness. Thin-wall theory is generally deemed valid when $H/t \geq 10$ (Seaburg and Carter, 1997). Thick-wall theory, which considers the shear stress gradient across the wall thickness, was used to derive the torsional inertia and modulus constants in Equations 15 and 16, respectively.

$$J_t = \frac{4tA_o^2}{p_m} + \frac{p_m t^3}{3} \tag{15}$$
$$= J + \frac{p_m t^3}{3}$$

$$C_t = \frac{J_t}{t + 2\frac{A_o}{p_m}} \tag{16}$$

The second term in Equation 15 is negligible, and the torsional inertia constant can be calculated with Equation 13 for all practical conditions. For box sections, the sectional properties can be calculated with $r_o = r_m = 0$.

## RESIDUAL STRESSES

Although residual stresses do not affect the torsional strength, the buckling strength is dependent on both the magnitude and the pattern of residual stresses. Also, serviceability rotations can be significantly higher than calculated if the residual stresses cause inelasticity prior to reaching the calculated yield moment.

### Cold-Formed HSS

Due to the cold-bending process, cold-formed square and rectangular HSS members have high through-thickness residual stresses at the corners. Liu et al. (2017) summarized the research on these residual stresses and determined that a mean value for the bending residual surface stress is 70% of the yield stress. This agrees well with the recommendations of Key et al. (1988) and Davison and Birkemoe (1983).

Longitudinal membrane residual stresses are compressive at the corners (Sherman, 1992). Measurements showed that these stresses are dependent to the HSS geometry, with values at the corners, flats, and weld approximately equal to 35%, 60%, and 70% of the yield strength, respectively (Zhang et al., 2016). Sherman (1971) developed a simplified pattern for cold-formed rectangular HSS members, where the longitudinal residual stresses varied linearly from 40% of the yield stress in compression at the corners to 40% of the yield stress in tension at the wall mid-width.

### Box Sections

For box sections, the longitudinal residual stresses at the corners are approximately equal to the plate yield stress. Depending on the plate width, compression residual stresses are between 10% and 30% of the yield stress. Compression residual stresses are nearly constant and cover most of the wall width. These characteristics have been verified for both fillet-welded sections (Uy, 1998; Ingvarsson, 1977; ECCS, 1976) and groove-welded sections (Chen and Chang, 1993).

### Hot-Formed HSS

Because the final cooling pattern is relatively uniform for hot-formed HSS members, residual stresses are usually considered negligible in buckling analysis (Sherman, 1992; ECCS, 1976). However, for the assumed pattern in ECCS, the residual stress varied linearly from 50% of the yield stress in compression at the corners to 20% of the yield stress in tension. For this pattern, the tension residual stress was constant over most of the wall width.

## BEHAVIOR

Rectangular HSS torsion members can fail by shear yielding, shear buckling, or cross-sectional collapse. The limit states that are applicable to common building members, shear yielding, and shear buckling will be discussed further in the remaining parts of this paper.

### Cross-Sectional Collapse

Cross-sectional collapse can occur when second-order effects cause the walls to deform inward at large torsional rotations as shown in Figure 2 (Chen, 2000). This cross-sectional flattening reduces the torsional strength, which causes an unstable post-buckling curve, resulting in collapse under large plastic deformations (Zaifuddin et al., 2017). Often identified as a distortional mode, the buckled shape is characterized by inward deformation at the wall mid-width (Chen, 2000; Chen and Wierzbicki, 2000; Zaifuddin et al., 2017), sometimes accompanied by inward deformation of the corners (Omidvari and Hematiyan, 2015). The length of diagonal half-waves along the member longitudinal axis are several times the half-wavelengths for

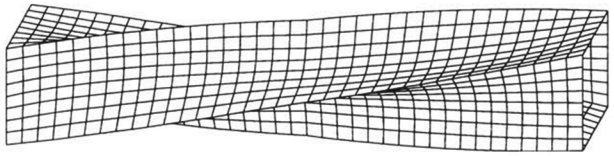

*Fig. 2. Cross-sectional collapse (Chen, 2000).*

the shear buckling mode, and they often extend over the full member length.

Because this limit state is applicable only when torsional rotations are significantly higher than the yield rotation, it is usually a consideration only for extreme loadings (such as for vehicle impact studies) and will not be addressed further in this paper. However, the unstable collapse behavior is a consideration for a reliability analysis that considers the consequences of failure. Also, the second-order effects in earlier loading stages can potentially affect the behavior by lowering the proportional limit torque.

### Shear Yielding

The shear yielding limit state is shown in Figure 3 (Chen, 2000). The behavior of rectangular HSS torsion members is similar to that of flexural members, where the moment-rotation curve is nonlinear. For a perfect flexural member with linear elastic–perfectly plastic material behavior, the moment-rotation curve is linear up to the yield moment, $M_y$. At higher moments, the curve is nonlinear up to the maximum value, which is the plastic moment, $M_p$. Figure 4 shows the torque versus twist plots for the specimens tested by Ridley-Ellis et al. (2003).

Because thick-wall theory considers the shear stress gradient across the wall thickness, the yield torsion can be calculated with Equation 17.

$$T_y = \tau_y C_t \tag{17}$$

Equation 18, which is based on thin-wall theory, is used to calculate the plastic torsion.

$$T_p = \tau_y C \tag{18}$$

For HSS sizes typically used in buildings, Ridley-Ellis (2000) determined that $T_p/T_y$ ranged between 1.05 and 1.25. Using the experimental data in Appendix A, the 20 specimens with an experimental failure mode of yielding had a mean torsional shape factor, $C/C_t$, of 1.12.

Figure 5 shows the data points for the experimental specimens that are documented in Appendix A, where $T_p/T_y$ is plotted versus the maximum overall wall width-to thickness ratio, $H/t$, with $H \geq B$. The plot shows a significant difference between the elastic and plastic properties when $H/t < 40$.

With flexural members, the moment-rotation curve becomes nonlinear at moments lower than $M_y$ due to stress concentrations, residual stresses, and geometric

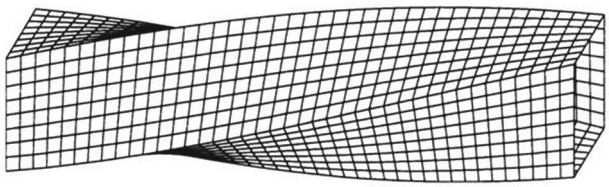

*Fig. 3. Shear yielding (Chen, 2000).*

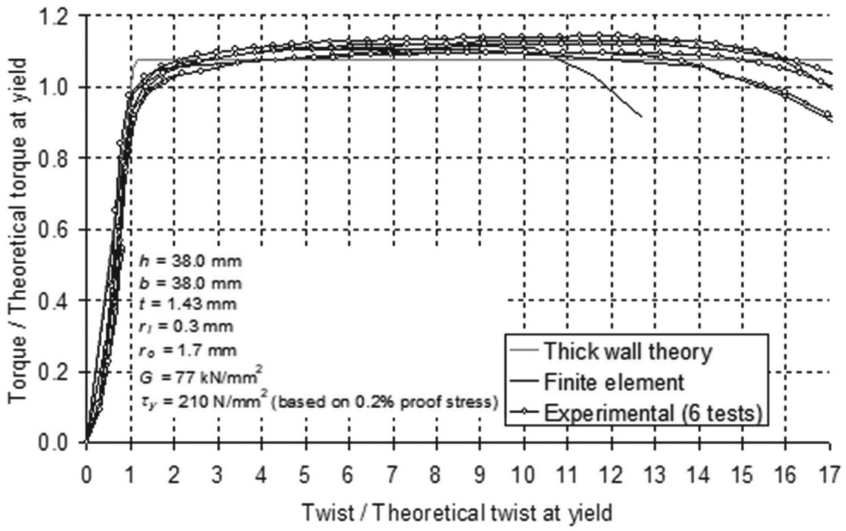


*Fig. 4. Torque versus twist for the specimens tested by Ridley-Ellis et al. (2003).*

imperfections. Rectangular HSS torsion members behave similarly, with residual stresses, geometric imperfections, and corner stress concentrations causing yielding at torques lower than $T_y$. Additionally, the proportional limit torque can be affected by cross-sectional collapse due to second-order flexural stresses in the walls.

### Shear Buckling

The shear buckling limit state is shown in Figure 6 (Zaifuddin et al., 2017). The critical stresses in AISC *Specification* Section H3.1 are identical to those calculated with the equations in AISC *Specification* Section G4. Section G4 defines the web shear buckling strength coefficient, $C_{v2}$, using the equations in Section G2.2, with a buckling coefficient, $k_v = 5.0$. Although the provisions of Chapter G were developed for beams that are subjected to direct shear, the Commentary to Section H3.1 discusses the similarities between direct shear and torsional shear: "The shear distribution due to torsion is uniform in the longest sides of a rectangular HSS, and this is the same distribution that is assumed to exist in the web of an I-shape beam. Therefore, it is reasonable that the provisions for buckling are the same in both cases." The design philosophy in Eurocode 3, Part 1-1 (CEN, 2005) Section 6.2.7 is similar to that of AISC *Specification* Section H3.1, with the critical shear stress calculated with the direct shear provisions in Eurocode 3, Part 1-5 (CEN, 2006).

### Warping

Theoretically, warping is not present in square HSS members or square box section members with constant wall thickness (Zyczkowski, 1991). Although corner details and geometric imperfections may affect the warping stresses, finite element models by Ridley-Ellis (2000) and experimental strain measurements by Konate (2015) showed that the warping stresses are negligible for these members.

Ridley-Ellis (2000) verified the presence of warping in rectangular HSS members and noted that the warping strains vary linearly across the width of the four walls. Warping strains are maximum at the corners and zero where a wall intersects a transverse axis of symmetry. Although warping is present in these members, it is common practice to neglect warping when designing rectangular HSS members for torsional loads. Ahlfors (2015) showed that this is conservative for the yielding limit state. For all practical aspect ratios, $H/B$, Derler and Unterweger (2021) showed that this practice is also conservative when the controlling limit state is buckling of the cross-sectional elements.

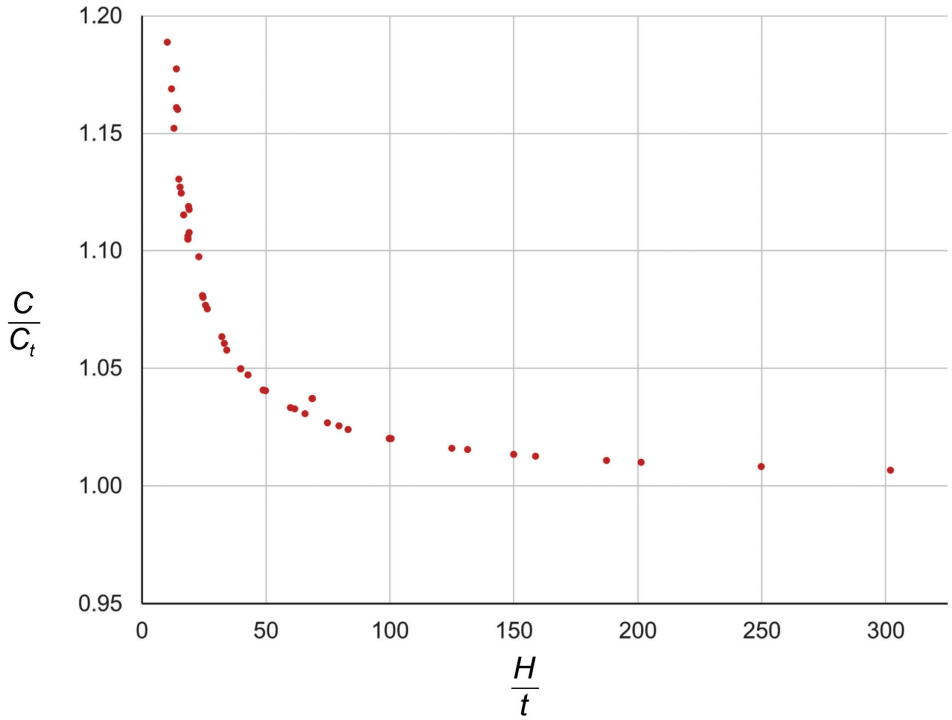


*Fig. 5. Graph of the torsional shape factor versus the overall wall slenderness for the experimental specimens.*

In some cases, it may be appropriate to consider the increased torsional resistance caused by warping for rectangular box sections with short lengths relative to the cross-sectional dimensions. Smith et al. (1970) provides information on analyzing the effects of warping in rectangular box sections. Also, including the warping stresses should be considered for a fatigue analyses (Ahlfors, 2015).

### Nonlinear Behavior

Nonlinear strength can result from stress redistribution, strain hardening, and post-buckling. Although significant nonlinear strength is available for the full range of wall slenderness values, utilization of the nonlinear range, whether characterized by gross inelastic yielding with strain hardening or post-buckling, can result in unacceptably large rotations of several times the yield rotation.

### Serviceability

When designing flexural members, properly designing for strength ensures that the serviceability design is accurate by limiting the moments to the linear portion of the moment-rotation curve. Beams are designed for deflection limits using serviceability loads and elastic sectional properties. For braced compact beams that are designed according to LRFD, $\phi_b M_p \le M_u$, where $\phi_b = 0.90$ and $M_u$ is the required flexural strength. As discussed in the Commentary to AISC *Specification* Section B3.1, LRFD is calibrated to ASD at a live-to-dead load ratio of 3.0. This results in an average LRFD load factor of 1.5 for live and dead load combinations. In this case, $M_p$ must be equal to or greater than $1.5/\phi_b = \Omega_b = 1.67$ times the maximum service moment for both ASD and LRFD. To ensure that the serviceability moments are limited to the linear portion of the moment-rotation curve, the combined effect of residual stresses and geometric imperfections must reduce $M_y$ by no more than $1/1.67$ times the shape factor, $Z_x/S_x$. This is the case for rolled W-shapes that are bent about the major axis. Although the typically minor detrimental effects of shear deformation and secondary load interaction are usually neglected in beam deflection calculations, potentially beneficial effects are also neglected. These include the partial end rotational restraint provided by typical shear connections, the stiffness of nonstructural building elements, and the higher expected yield stress relative to the specified minimum value.

Although serviceability rotations for torsion members are calculated in a manner that is analogous to the calculation of beam deflections, it is unclear if the serviceability torques are on the linear portion of the torque-rotation curve. Rectangular HSS sections typically have high residual stresses at the weld seam and cold-bending residual stresses at the corners. This, combined with the stress concentrations at the corners and second-order effects can cause yielding at torques significantly lower than $T_y$.

## HISTORICAL REVIEW

This part of the paper provides a review of the existing research on square and rectangular hollow section members that are subjected to torsion. Experimental tests that were included in the reliability analysis are discussed as well as the relevant research on shear buckling and residual stresses.

### Hovgaard (1937)

Hovgaard (1937) documented the torsional tests of three rectangular tubes of drawn and annealed mild steel. The shear strains were measured at several locations on the cross section. The measured torsional rotations "showed fair agreement with theory" in the elastic range. However, the torque-rotation curves became nonlinear at torques less than the calculated yield torques, $T_c = 0.6\sigma_y C$, where $\sigma_y$ is the measured uniaxial tension yield stress.

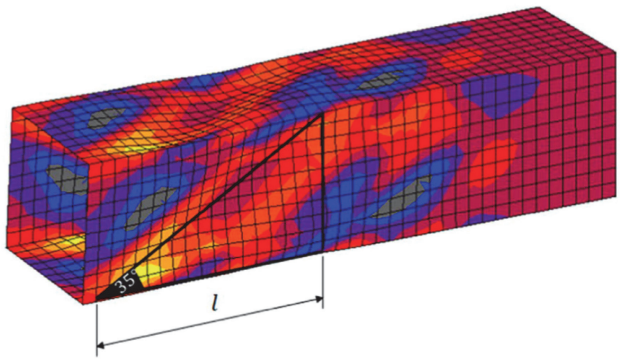


*Fig. 6. Shear buckling (Zaifuddin et al., 2017).*

Specimen C was $3 \times 3 \times 0.070$ in. $\times$ 52 in. long, with $\sigma_y$ = 24.0 ksi. Nonlinear behavior initiated at a torque of only 75% of the theoretical yield torque.

Specimen D was $6 \times 3 \times 0.313$ in. $\times$ 51 in. long, with $\sigma_y$ = 35.5 ksi. Nonlinear behavior initiated at a torque of only 49% of the theoretical yield torque.

Specimen E was $4 \times 4 \times 0.192$ in. $\times$ 51 in. long, with $\sigma_y$ = 26.0 ksi. Because this test was used primarily to accurately determine the stress distribution, it was loaded only in the linear range. The measured torsional rotation was 87% of the calculated value. The measured shear stresses were higher than average near the corners.

**Peters (1954)**

Peters (1954) recognized that the HSS wall shear stresses caused by torsional loading are similar to the stresses caused by direct shear. He compared the theories for buckling of long flat plates with the results of elastic and plastic buckling tests on long square tubes loaded in compression, torsion, and combined compression and torsion. It was determined that the torsional loading direction has little to no effect on the shape of the interaction curve. Peters recommended a design procedure based on the classical shear buckling equation, where the elastic critical stress is multiplied by a plasticity reduction factor. The elastic critical stress, $\tau_{e,}$ of an infinitely long plate with simply supported edges subjected to shear is calculated with Equation 5.

**Basler (1963)**

An empirical transition curve between shear yielding and elastic buckling was proposed by Basler (1963). He observed a proportional limit at 80% of the shear yield stress: $\tau_p = 0.8\tau_y$. For stresses greater than the proportional limit, the inelastic buckling stress is

$$\tau_{cr} = \sqrt{\tau_p \tau_e} = \sqrt{0.8\tau_y \tau_e} \tag{19}$$

Equation 19 can be used to derive AISC *Specification* Equation G2-4.

$$C_{v1} = \frac{\tau_{cr}}{\tau_y} = \sqrt{\frac{0.8\tau_e}{\tau_y}} = \sqrt{\frac{0.8}{\tau_y}\frac{\pi^2 k_v E}{12(1-\nu^2)(h/t)^2}} = \frac{1.10\sqrt{k_v E/F_y}}{h/t} \tag{20}$$

Substituting $k_v$ = 4.96 into Equation 20 results in Equation 21, where the web shear strength coefficient produces the same shear strength as AISC *Specification* Equation H3-4.

$$C_{v1} = \frac{2.45\sqrt{\frac{E}{F_y}}}{\left(\frac{h}{t}\right)} \tag{21}$$

**Wittrick and Curzon (1968)**

Wittrick and Curzon (1968) developed stability functions for the buckling strength of square HSS members subjected to torsion and solved the equations iteratively to determine appropriate buckling coefficients. Although the corners remained straight, buckling caused corner rotations, inducing interaction between adjacent walls. The buckling mode was characterized by continuous two-start spirals advancing by one complete wavelength for each revolution of the member. The buckling half-wavelength is 1.24*H*. The buckling coefficient is 5.3395, which is almost identical to the value that was derived by the authors for an infinitely long simply supported plate: 5.336.

**Marshall (1970, 1971, 1972)**

Marshall (1970) derived approximate equations for thick-walled rectangular hollow sections without corner radii. He noted that thin-wall theory predicts stresses with 12% nonconservative error for sections with $B/t$ = 20, and the error "gets rapidly worse for thicker sections."

Marshall (1971) expanded the solution of Marshall (1970) to include corner radii. The equations were solved numerically, using the finite difference method.

Nine square and rectangular HSS torsion specimens were tested by Marshall (1971, 1972). All specimens were 4.5 ft long. The outside dimensions were 1.5, 2.0, 2.5, 3.0, 4.0, and 5.0 in. The wall thicknesses were 0.128, 0.160, 0.192, and 0.250 in. The measured uniaxial tension yield stresses, $\sigma_y$, were 44.57 and 62.71 ksi. All specimens were loaded until the strain hardening region was reached.

Comparisons with the experimental results showed that thin-wall theory underpredicts the shear stresses by an average of 14.2%. The measured torsional rotations were in reasonable agreement with the calculated rotations in the elastic range. Both the experimental results and the numerical models showed significant stress concentration at the corners; however, the areas of elevated stress covered less than 1% of the cross-sectional area.

**Kitada et al. (1989)**

Kitada et al. (1989) tested seven box sections with various combinations of axial compression, flexure, and torsion. Only one specimen was subjected solely to torsion. The specimens were 450 mm (17.7 in.) long. The outer dimensions were 133 mm (5.24 in.) × 163 mm (6.42 in.), and the plates were 4.5 mm (0.177 in.) thick. The initial out-of-flatness of the walls was approximately equal to 1/150 of the plate width. The measured uniaxial tension yield stresses, $\sigma_y$, was 289 N/mm$^2$ (41.9 ksi). The experimental-to-calculated strength ratio was 1.04, where the calculated yield torque is $T_c = 0.6\sigma_y C$.

**Mahendran and Murray (1990)**

Mahendran and Murray (1990) tested 54 built-up hollow square sections in various combinations of axial compression and torsion. Sixteen of the specimens were subjected solely to torsion. The section was formed of two elements that were cold bent at the corners. The two elements were connected by spot welding at the corners to form a hollow square section. The outer dimension was 151 mm (5.94 in.), and the thickness ranged from 0.500 mm (0.0197 in.) to 2.45 mm (0.0965 in.). This resulted in $h/t$ ratios between 60 and 300. The measured uniaxial tension yield stresses, $\sigma_y$, were 220 MPa (31.9 ksi) and 285 MPa (41.3 ksi).

The buckled specimens had waves that were inclined at approximately 30° to the longitudinal member axis. The authors noted that the presence of initial geometric imperfections "did not seem to have a significant effect" on the strength.

**White et al. (1993)**

White et al. (1993) tested built-up hollow square sections in various combinations of axial compression and torsion. Five of the specimens were subjected solely to torsion. The "closed-hat" section was formed of two elements, with a cold-bent U-shaped element and a flat plate element. The two elements were connected by spot welding at 20 mm (0.79 in.) intervals to form a hollow square section. The outer dimension was 50 mm (2.0 in.), and the thickness ranged from 0.38 mm (0.015 in.) to 1.5 mm (0.059 in.). This resulted in $h/t$ ratios between 31 and 130. The material was "cold-rolled automotive grade steel sheet," with measured uniaxial tension yield stresses, $\sigma_y$, between 269 MPa (39.0 ksi) and 590 MPa (85.6 ksi).

For the specimens with low $h/t$ ratios, the experimental strengths were slightly overpredicted when the calculated strength was based on thin-wall theory. In this case, the calculated strength is $T_c = 0.6\sigma_y C$. For the specimens with high $h/t$ ratios, the experimental strength was predicted with reasonable accuracy using Equation 5 to calculate the elastic critical shear stress with $k_v = 5.35$.

**Ridley-Ellis et al. (2003)**

Ridley-Ellis et al. (2003) tested five square and rectangular HSS members subjected to torsion. All specimens were 2,000 mm (78.7 in.) long. The specified outside dimensions were 100, 150, and 200 mm (3.9, 5.9, and 7.9 in.). The wall thicknesses were 6.3 and 8 mm (0.25 and 0.32 in.). The shapes were manufactured and "hot-finished" by either British Steel Tubes/Corus or Vallourec and Mannwsmann Tubes. Because the specimens were normalized after forming, the residual stresses were expected to be significantly lower than for a typical cold-formed HSS section. The materials were either S275 or S355, with measured uniaxial tension yield stresses, $\sigma_y$, between 329 MPa (47.7 ksi) and 405 MPa (58.7 ksi).

All specimens were loaded into the plastic range without buckling. For S275 and S355 HSS, the maximum experimental torques were approximately 20% and 12% lower than the strengths calculated with thin-wall theory, respectively. In this case, the calculated strength is $T_c = 0.6\sigma_y C$. They determined that "the experimentally measured torque-twist relationships differ significantly from the theoretical predictions," when thin-wall theory was used. The authors recommended thick-wall theory for design because it results in calculated strengths and stiffnesses that are more consistent with the experimental results and finite element models.

**Kim and Yoo (2008)**

Kim and Yoo (2008) studied box sections using finite element models that were subjected to various combinations of flexure and torsion. Width-to-thickness ratios of 20, 40, and 80 were used to simulate elastic, inelastic, and plastic behavior. Welding residual stresses were modeled using a simplified pattern made up of rectangular stress blocks. At the corners, tensile residual stresses were equal to the yield stress. The remaining wall width had compressive residual stresses equal to 20% of the yield stress.

By curve fitting the results of 64 models that were subjected to torsional loads, the authors developed Equation 22 to calculate the torsional strength ratio based on the wall slenderness. The range of validity for Equation 22 is $0.7 < \lambda_T < 2$.

$$\alpha = \frac{T_n}{T_p} = \frac{F_{cr}}{\tau_y} = 0.78 + 0.71\lambda_T - 0.85\lambda_T^2 + 0.22\lambda_T^3 \quad (22)$$

**Belingardi et al. (2008)**

Belingardi et al. (2008) tested 10 built-up hollow square sections in torsion. The section was formed of two hat or C-shaped elements that were cold bent at the corners. The two elements were connected by either spot welding or adhesive bonding of the lap joints on opposite walls to form a hollow square section. The outer dimension was 40 mm

(1.57 in.), and the thickness was 1.00 mm (0.0394 in.). This resulted in $h/t = 36$. The low carbon sheet steel had a measured uniaxial tension yield stress, $\sigma_y$, of 210 MPa (30.5 ksi).

After the specimens reached the elastic limit torques, approximately 15% to 30% more strength was available; however, this post-yield strength was accompanied by large rotations. At large rotations, cross-sectional collapse occurred, where the walls deformed inward.

**Chahkand et al. (2013)**

In addition to carbon fiber reinforced polymer (CFRP)-reinforced specimens, Chahkand et al. (2013) tested two non-reinforced square HSS specimens that were subjected to torsion. The specified outside dimension for all specimens was 50 mm (2.0 in.), and the specified wall thickness was 3 mm (0.12 in.). This resulted in an $h/t$ ratio of 15.5. The hot-formed shapes had a measured uniaxial tension yield stress, $\sigma_y$, of 382 MPa (55.4 ksi). Due to the low $h/t$ ratio, the specimens exhibited a stable post-yield curve, with increased strength caused by strain hardening.

**Goncalves and Camotim (2013)**

Using finite element models of square HSS members, Goncalves and Camotim (2013) showed that the buckling strength increases with decreasing member length; however, significant increases are applicable only for $L/H < 3$. For $L/H = 10$, the results were within 2% of those for infinitely long members. The authors developed buckling coefficients of 5.444 and 5.390 for $L/H = 10$ using different modeling techniques; however, they noted that $k_v = 5.34$ is an appropriate lower-bound design value.

**Omidvari and Hematiyan (2015)**

Using a parametric finite element study, Omidvari and Hematiyan (2015) showed that two buckling modes exist for rectangular HSS torsion members. For members with very high $h/t$ ratios, the first mode is similar to plate shear buckling, where the deformation of the HSS corners is negligible.

Members with lower $h/t$ ratios, which more closely represent the HSS members used in building structures, have a distortional first buckling mode. The distortional mode is characterized by considerable inward deformation of the corners and diagonal waves along the member length that are several times the half-waves for the shear buckling mode. This mode is applicable in the inelastic range, which is generally accepted to be the range between 80% and 100% of the yield strength due to material and geometric imperfections (Basler, 1963).

Curve fit equations were developed from the finite element models to predict the distortional buckling stress. Equation 23 is a simplified version of the equations with an applicability range of $h_o/t \geq 50$.

$$\tau_e = 24.1G\frac{t^2}{h_o(h_o + b_o)} \tag{23}$$

where $h_o = H - t$, $b_o = B - t$, and $h_o \geq b_o$.

**Konate (2015)**

Konate (2015) tested 60 HSS1.5×1.5×⅛ in. members in various combinations of flexure, axial compression, and torsion. Only two of the specimens were subjected solely to torsion. All specimens were 34 in. long. The measured uniaxial tension yield stress, $\sigma_y$, was 59.0 ksi.

Strain gages were used to measure the longitudinal strains that were induced by warping. Because the measured strains were between 1.35% and 5.52% of the yield strains, the authors concluded that the warping stresses are negligible.

The analysis used a yield torque based on the limiting shear stress calculated with Equation 24, where $\sigma_r$ is the maximum longitudinal residual stress. For the simplified residual stress pattern that was used in the analysis, $\sigma_r = 0.5\sigma_y$, resulting in $\tau_{yr} = 0.5\sigma_y = 0.87\tau_y$.

$$\tau_{yr} = \sqrt{\frac{\sigma_y^2 - \sigma_r^2}{3}} \tag{24}$$

**Sharrock et al. (2015)**

In addition to aluminum and CFRP-reinforced specimens, Sharrock et al. (2015) tested six non-reinforced steel square HSS specimens that were subjected to torsion. The specified outside dimension for all specimens was 100 mm (3.9 in.). The specified wall thicknesses were 2, 3, and 6 mm (0.079, 0.12, and 0.24 in.). This resulted in $h/t$ ratios of 11.9, 30.3, and 44.9, respectively. The cold-formed shapes were manufactured by One Steel Tube Mills. The material was C450PLUS, with measured uniaxial tension yield stresses, $\sigma_y$, between 383 MPa (55.5 ksi) and 444 MPa (64.4 ksi).

Shear buckling in the specimens with 2 and 3 mm wall thickness caused a "dramatic drop in the torsional capacity" at torsional rotations of approximately 5° and 10°, respectively. Buckling did not occur in the specimens with 6 mm wall thickness. These specimens reached at least 20° rotations prior to significant reductions in the strength.

**Chen (2016)**

A finite element study by Chen (2016) showed buckling waves inclined at approximately 30° to the longitudinal member axis. Based on this, a plate buckling coefficient of $k_v = 5.35 + [2\tan(30°)]^2 = 6.68$ was recommended.

**Zaifuddin et al. (2017)**

For square HSS, finite element models developed by Zaifuddin et al. (2017) showed buckling waves inclined at approximately 35° to the longitudinal member axis. This angle was essentially constant for all models regardless of the width-to-thickness ratio. Based on this, a plate buckling coefficient of $k_v = 5.35 + [2\tan(35°)]^2 = 7.31$ was recommended.

**Rendall et al. (2018)**

A study of square HSS members using the finite strip method by Rendall et al. (2018) resulted in a buckling half-wavelength of $1.24H$ and a buckling coefficient of 5.3396, which is almost identical to the values determined by Wittrick and Curzon (1968).

**Devi et al. (2019)**

In addition to tests of HSS members with circular openings in the walls, Devi et al. (2019) tested two square HSS torsion specimens without openings. Additionally, finite element models were used to determine the behavior of members with various wall slenderness ratios. The specified outside dimension for the experimental specimens was 60 mm (2.4 in.), and the specified wall thickness was 3.2 mm (0.13 in.). For the finite element models, the specified outside dimension was 150 mm (5.9 in.), and the specified wall thicknesses varied from 0.6 to 10 mm (0.024 to 0.39 in.). This resulted in $h/t$ ratios that varied from 11 to 250. The specimens were cold formed, with a measured uniaxial tension yield stress, $\sigma_y$, of 412 MPa (59.8 ksi).

The authors developed a method to calculate the rotation capacity based on the wall slenderness. Empirical equations were then developed to calculate the strength based on the rotation capacity ratio. Both their proposed deformation-based method and the AISC *Specification* equations provided accurate predictions for the torsional strength.

## RELIABILITY ANALYSIS

In this part of the paper, a first-order reliability analysis will be used to calculate appropriate resistance factors for use with AISC *Specification* Equation H3-1. The resistance factor required to obtain a specific reliability level is (Galambos and Ravinda, 1978).

$$\phi = C_R \rho_R e^{-\beta \alpha_R V_R} \tag{25}$$

where

$C_R$ = correction factor
$V_R$ = coefficient of variation
$\alpha_R$ = separation factor
$\beta$ = reliability index
$\rho_R$ = bias coefficient

Galambos and Ravinda (1973) proposed a separation factor, $\alpha_R$, of 0.55. For $L/D = 3.0$, Li et al. (2007) developed Equation 26 for calculating the correction factor.

$$C_R = 1.40 - 0.156\beta + 0.0078\beta^2 \tag{26}$$

Based on the Commentary to *Specification* Section B3.1, the target reliability index, $\beta_T$, is 2.6, which results in $C_R = 1.05$. The reliability analysis also includes calculations using $\beta_T = 3.0$, which results in $C_R = 1.00$. The coefficient of variation and bias coefficient are calculated using the statistical parameters of the specific joint. The bias coefficient is

$$\rho_R = \rho_M \rho_G \rho_P \tag{27}$$

where

$\rho_G$ = bias coefficient for the geometric properties
$\rho_M$ = bias coefficient for the material properties
$\rho_P$ = bias coefficient for the test-to-predicted strength ratios; mean value of the professional factor calculated with the measured geometric and material properties

The coefficient of variation is

$$V_R = \sqrt{V_M^2 + V_G^2 + V_P^2} \tag{28}$$

where

$V_G$ = coefficient of variation for the geometric properties
$V_M$ = coefficient of variation for the material properties
$V_P$ = coefficient of variation for the test-to-predicted strength ratios

**Material and Geometric Parameters**

Osterhof and Driver (2011) used $\rho_t = 1.00$ and $V_t = 0.050$ for the thickness characteristics of HSS shapes. For ASTM A500 Grade C HSS shapes, Dowswell (2021) calculated $\rho_t = 0.994$ and $V_t = 0.00710$. For plates, Hess et al. (2002) recommended $\rho_t = 1.05$ and $V_t = 0.044$, and Schmidt and Bartlett (2002) recommended $\rho_t = 1.04$ and $V_t = 0.025$.

The author was unable to locate statistical data regarding deviations from the specified overall height and width of HSS shapes. However, for members meeting ASTM A500 and A1085 tolerances, any variation of the overall dimensions results in only a 2% worst-case strength reduction. Additionally, extensive statistical data related to HSS corner radii are unavailable. Packer and Frater (2005) and Gong (2008) measured corner radii of HSS flare bevel weld specimens, resulting in $r_o/t$ ratios between 1.78 and 2.43. Comparison of the torsional modulus constants for HSS

shapes with various $r_o/t$ ratios calculated with Equation 10 indicate that the variability of the corner radii is negligible. When both the overall dimensions and corner radii are considered deterministic quantities, $\rho_G$ and $V_G$ are dependent only on the wall thickness, $t$.

Depth variations for welded structural members are in AWS D1.1 (2020) Subclause 7.22.9. The maximum underrun is ⅛ in. for depths up to and including 36 in. and 3⁄16 in. for depths over 36 in. Schmidt and Bartlett (2002) compiled actual-to-specified ratios for welded built-up I-shaped members, with mean flange width and overall depth ratios of 0.998 and 0.999, respectively. Because the torsional strength reduction is insignificant for these values, the overall dimensions are considered a deterministic quantity. For these conditions, $\rho_G$ and $V_G$ are dependent only on the wall thickness, $t$.

The material characteristics for modulus of elasticity are $\rho_E = 1.04$ and $V_E = 0.045$ for HSS shapes and $\rho_E = 1.04$ and $V_E = 0.026$ for plates (Schmidt and Bartlett, 2002). For plates, Hess et al. (2002) recommended $\rho_E = 0.987$ and $V_E = 0.076$.

Dowswell (2021) summarized the tensile strengths parameters from five HSS research projects (Zhao et al., 2008; Han et al., 2007; Yang and Mahin, 2005; Zhao et al., 1999; Zhao and Hancock, 1995). For these tests, coupons were extracted from the flat portions of the walls of ASTM A500 Grade B, A500 Grade C, and similar international grades. Using 20 data points from these papers, the yield strength parameters were calculated, resulting in $\rho_M = 1.20$ and $V_M = 0.0686$.

Liu et al. (2007) reported the material characteristics for the yield stress of rectangular HSS shapes manufactured according to ASTM A500 Grade B to be $\rho_y = 1.31$ and $V_y = 0.08$. However, these values are based on only one of the eight approved material grades listed in AISC *Specification* Section A3.1 for rectangular HSS shapes. Also, AISC *Manual* (2023) Table 2-4 designates ASTM A500 Grade C as the preferred HSS material specification. Therefore. the more conservative values from Schmidt and Bartlett (2002) may be more appropriate: $\rho_y = 1.18$ and $V_y = 0.063$.

Brockenbrough (2001) reported the material characteristics for ASTM A36, A514, A572 Grade 50, A572 Grade 60, A572 Grade 65, A588, and A852 plates. The mean values were $\rho_y = 1.18$ and $V_y = 0.063$. The lowest bias coefficient was $\rho_y = 1.11$ with $V_y = 0.06$ for A588 plates with 2 in. $< t \leq$ 4 in. When the A36 plates are excluded from the data set, the mean values were $\rho_y = 1.16$ and $V_y = 0.064$.

Schmidt and Bartlett (2002) reported the material characteristics for the yield stress of plates based on the thickness. The mean values were $\rho_y = 1.11$ and $V_y = 0.056$. The lowest bias coefficient was $\rho_y = 1.07$ with $V_y = 0.054$ for plates less than 30 mm (1.2 in.) thick. $\rho_y$ increased with thickness up to a maximum value of 1.16 for plates between 40 and 50 mm.

For "high-strength" steels, which had a mean measured yield stress of 49.6 ksi, Hess et al. (2002) recommended $\rho_y = 1.19$ and $V_y = 0.083$. For ASTM A572 and A588 Grade 50 plates, Suwan et al. (2003) reported $\rho_y = 1.16$ and $V_y = 0.0637$.

Liu et al. (2007) reported the material characteristics for ASTM A36, A529 Grade 50, A529 Grade 55, A572 Grade 50, and A572 Grade 55 plates. The mean values were $\rho_y = 1.20$ and $V_y = 0.06$. The lowest bias coefficient was $\rho_y = 1.10$ with $V_y = 0.05$ for A529 Grade 55 plates. For the four groups with only A529 and A572 plates, $\rho_y = 1.15$ with $V_y = 0.06$.

The reliability analysis must be based on the three equations for yielding (H3-3), inelastic buckling (H3-4), and elastic buckling (H3-5). For a first-order multivariate analysis, the mean and variance of $T_c$ can be approximated with Equations 29 and 30, respectively (Benjamin and Cornell, 1970).

$$T_{cm} \approx f(X_{1m}, X_{2m}, ..., X_{nm}) \tag{29}$$

$$\sigma_{T_c}^2 \approx \sum_{i=1}^{n} \left( \left[ \frac{\partial T_c}{\partial X_i} \right]_m \right)^2 \sigma_{X_i}^2 \tag{30}$$

where

$T_c$ = critical torsional strength, kip-in.
$T_{cm}$ = mean value of the critical torsional strength, kip-in.
$X_i$ = uncorrelated variables affecting $T_c$

Substituting Equations H3-3 and 10 into Equation H3-1, the critical torsional strength for the limit state of yielding is

$$T_c = 1.2 F_y t A_o \tag{31}$$

Because Equation 31 is linear with respect to both $F_y$ and $t$, the statistical parameters for the material and geometric properties are used without manipulation as listed in the third column of Table 1.

Substituting Equations H3-4 and 10 into Equation H3-1, the critical torsional strength for the limit state of inelastic buckling is

$$T_c = 2.94 \sqrt{E F_y} \frac{A_o t^2}{h} \tag{32}$$

The derivative of $T_c$ with respect to $E$ is

$$\frac{\partial T_c}{\partial E} = \left( \frac{1}{2} \right) 2.94 \sqrt{\frac{F_y}{E}} \frac{A_o t^2}{h} \tag{33}$$

The derivative of $T_c$ with respect to $F_y$ is

$$\frac{\partial T_c}{\partial F_y} = \left( \frac{1}{2} \right) 2.94 \sqrt{\frac{E}{F_y}} \frac{A_o t^2}{h} \tag{34}$$

| Table 1. Reliability Functions | | | | |
|---|---|---|---|---|
| | | | Buckling | |
| | | Yielding | Inelastic | Elastic |
| Material | $\rho_M$ | $\rho_y = 1.15$ | $(\rho_E\rho_y)^{½} = 1.09$ | $\rho_E = 1.04$ |
| | $V_M$ | $V_y = 0.06$ | $V_E/2 + V_y/2 = 0.053$ | $V_E = 0.045$ |
| Geometric | $\rho_G$ | $\rho_t = 0.994$ | $(\rho_t)^2 = 0.988$ | $(\rho_t)^3 = 0.982$ |
| | $V_G$ | $V_t = 0.04$ | $(2)(V_t) = 0.08$ | $(3)(V_t) = 0.12$ |

| Table 2. Statistical Parameters for Test-to-Predicted Strength Ratios Using the AISC *Specification* Section H3 Equations | | | | | |
|---|---|---|---|---|---|
| | | | Buckling | | |
| | All | Yielding | All | Inelastic | Elastic |
| $N$ | 48 | 30 | 18 | 2 | 16 |
| $\rho_P$ | 1.23 | 0.922 | 1.74 | 0.831 | 1.85 |
| $V_P$ | 0.621 | 0.118 | 0.607 | 0.145 | 0.575 |
| $N$ = number of specimens | | | | | |

The derivative of $T_c$ with respect to $t$ is

$$\frac{\partial T_c}{\partial t} = (2)2.94\sqrt{EF_y}\frac{A_o t}{h} \tag{35}$$

The statistical parameters for the geometric and material properties for inelastic buckling are listed in the fourth column of Table 1. Substituting Equations H3-5 and 10 into Equation H3-1, the critical torsional strength for the limit state of elastic buckling is

$$T_c = 9.04E\frac{A_o t^3}{h^2} \tag{36}$$

Equation 36 is linear with respect to $E$. The derivative of $T_c$ with respect to $t$ is

$$\frac{\partial T_c}{\partial t} = (3)9.04E\frac{A_o t^2}{h^2} \tag{37}$$

The statistical parameters for the geometric and material properties for elastic buckling are listed in the fifth column of Table 1.

## Professional Factors

The statistical parameters for the test-to-predicted strength ratios were calculated using 48 experimental tests from 11 research projects described previously in this paper. Of the research discussed in the historical review, only the experiments with adequate data were included in the analysis. This included tests by Marshall (1972), Kitada et al. (1989), Mahendran and Murray (1990), Al-Ayish (2004), White et al. (1993), Ridley-Ellis et al. (2003), Belingardi et al. (2008), Chahkand et al. (2013), Sharrock et al. (2015), Konate (2015), and Devi et al. (2019). The specimen details and experimental results are listed in Appendix A, Tables A1 and A2, respectively. Mahendran and Murray (1990) Specimen 6 was omitted from the data set because $h/t = 300$, which exceeds the AISC *Specification* limit of 260.

Because the reliability functions are separated into three groups (yielding, inelastic buckling, elastic buckling), each group was analyzed separately. Statistical parameters for test-to-predicted strength ratios, $\rho_P$ and $V_P$, as well as the number of specimens, $N$, within each group are listed in Table 2.

## Analysis

From Table 2, $\rho_P = 1.23$ when the AISC *Specification* equations are used with all specimens. Without further consideration, this appears reasonable. However, when the yielding and buckling limit states are considered separately, inconsistencies are revealed. For yielding, $V_P = 0.118$ is reasonable; however, $\rho_P = 0.922$ is significantly less than 1.00. For buckling, $\rho_P = 1.74$ is significantly greater than 1.00, and $V_P = 0.607$ indicates that the design model is inaccurate.

With $\phi = 0.90$, the *Specification* equations result in $\beta = 2.63$ for the 30 specimens with a predicted failure mode of yielding. With $\beta_T = 2.6$, $\phi = 0.906$. With $\beta_T = 3.0$, $\phi = 0.841$.

With $\phi = 0.90$, the *Specification* equations result in $\beta = 2.47$ for the 16 specimens with a predicted failure mode of elastic buckling. With $\beta_T = 2.6$, $\phi = 0.853$. With $\beta_T = 3.0$, $\phi = 0.716$.

### Discussion

Figure 7 shows a graph of $T_e/T_y$ versus $\lambda$ for the experimental data. $T_e$ is the maximum experimental torsional moment. $T_y$ is the torsional yield moment calculated with the measured specimen geometry and the measured uniaxial yield stress: $T_y = 0.6\sigma_y C$. The slenderness parameter, $\lambda$, is calculated with Equation 38. For the calculation of $\lambda$ for the experimental data points, the measured dimensions and material properties were used in lieu of the nominal values.

$$\lambda = \frac{h}{t}\sqrt{\frac{\sigma_y}{E}} \tag{38}$$

The AISC *Specification* curve is inaccurate over most of the buckling range, with excessive conservatism when $\lambda > 4$ and a nonconservative range when $1.5 < \lambda < 3$. The accuracy and transition (anchor) points of AISC *Specification* Equations H3-4 and H3-5 can be improved by addressing the sources of error in the design model.

In AISC *Specification* Section H3.1, the definition of $h$ is inaccurate. Because the buckled shape is usually characterized by buckling of all four walls, the interaction between walls should be considered. This can be accomplished by defining the buckling width as the larger of the two midwall-to-midwall distances for pairs of opposite walls (i.e., $h_o = H - t$ in Figure 1).

Equation 11 was derived using thin-wall theory, which is based on the assumption that the shear stress is constant across the wall thickness. However, the experimental results indicate that thin-wall theory results in overestimates of the torsional strength. Equation 16, which was derived using thick-wall theory, is more accurate that Equation 11.

## DISCUSSION AND RECOMMENDATIONS

This part of the paper discusses potential improvements to the AISC *Specification* design method. Revised design equations are proposed, and the reliability of the new design method is analyzed. Serviceability considerations are also discussed.

### Section Properties

As discussed previously in this paper, the yield and plastic torsion properties can be calculated with thick- and thin-wall theory, respectively. The differences in the elastic and plastic section properties are on the same order as for the flexural design of common I-shaped members (Ridley-Ellis, 2000). Therefore, for a highly refined torsional design method, a linear transition between the plastic and elastic strengths could be implemented. However, a review of the experimental data points on the yield plateau of Figure 2 indicate that a more refined method may

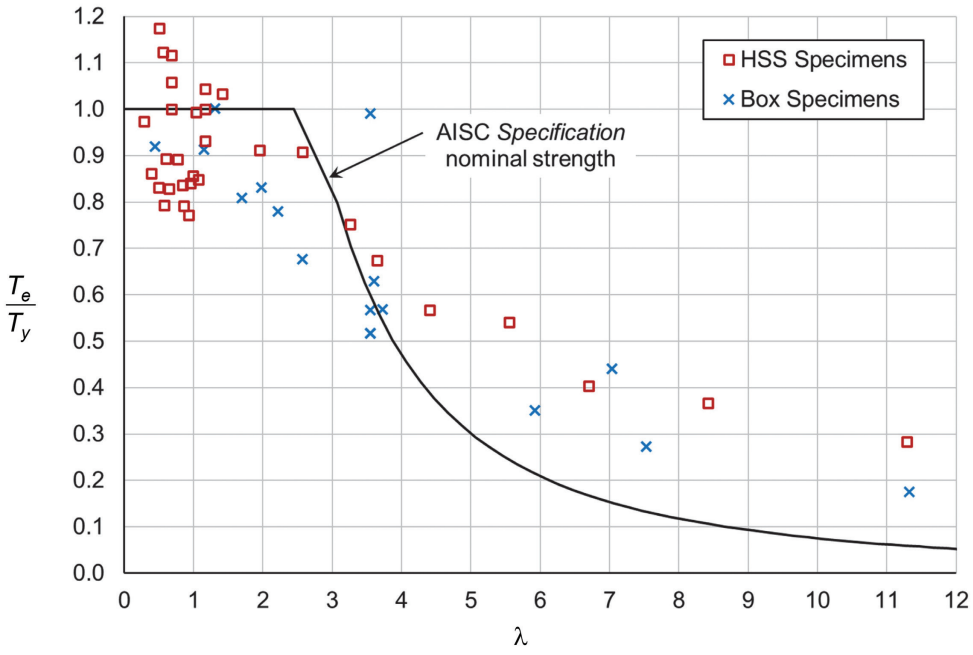


*Fig. 7. Graph of AISC equations with experimental data.*

not be justified. This is because, for the 20 specimens with an experimental failure mode of yielding, the data trend is relatively constant in the range $0 \le \lambda \le 1.5$. For $\lambda > 1.5$, the AISC *Specification* equations should be revised to include the effect of buckling.

The reliability analysis shows that the yield strength bias coefficient offsets the slightly nonconservative nature of using section properties calculated with thin-wall theory over the entire yielding plateau. Therefore, it is recommended that Equation 11 is used to calculate the torsional modulus constant, $C$, for HSS members. For box sections, the sectional properties can be calculated using Equation 10 with $r_m = 0$.

Equation 12, which was derived using the maximum permissible outside corner radius, results in slightly lower values for $C$. However, the difference between Equations 11 and 12 is negligible for most HSS shapes. Also, measurements by Packer and Frater (2005) and Gong (2008) showed that the outside corner radius is closer to 2 times the wall thickness, which was assumed in the derivation of Equation 11.

### Wall Buckling

The experimental data clearly showed that the wall buckling model should be based on a buckling width, $h_o$, defined as the largest distance between the mid-thickness of adjacent walls. The research of Wittrick and Curzon (1968), Goncalves and Camotim (2013), Chen (2016), Zaifuddin et al. (2017), and Rendall et al. (2018) indicated that a buckling coefficient of $k_v = 5.34$ is appropriate for use in Equation 5. Equation 42 was derived by substituting Equation 5 into Equation 4 with $k_v = 5.34$ and $h_o$ replacing $h$.

Figure 7 clearly shows that the yield plateau in the current AISC *Specification* design model should be shortened. Theoretically, this can be accomplished by revising the assumed residual stresses and geometric imperfections. Although research data are available to quantify the residual stresses, their magnitudes and patterns vary significantly between the various sections due to the different manufacturing and fabrication processes. Because the experimental specimens in the database included all common manufacturing and fabrication processes, the best-fit curve can be established first, and then the implied effect of imperfections can be calculated based on the intersection of the yield and buckling curves.

After the yielding-buckling anchor point is established, the shape of the curve can be adjusted to improve the accuracy of the design model. The inelastic and elastic buckling curves can be replaced by a single nonlinear curve that simplifies the design process. Equation 41 is of the form that was proposed by Devi et al. (2019); however, the constants were adjusted to result in similar reliabilities for the yielding and buckling limit states.

### Proposed Design Method

AISC *Specification* Section H3 is limited to HSS shapes. The proposed design method is applicable to both HSS and box section members. The proposed method uses *Specification* Equation H3-1 and replaces Equations H3-3, H3-4, and H3-5 with Equations 39, 40, and 41.

The nominal torsional strength of an HSS or box section member is calculated with Equation H3-1 in AISC *Specification* Section H3.1.

$$T_n = F_{cr}C \qquad \text{(AISC } Spec. \text{ H3-1)}$$

For rectangular HSS and box section members, the critical shear stress is

$$F_{cr} = 0.6F_yC_v \tag{39}$$

When $\lambda_T \le 0.530$

$$C_v = 1.00 \tag{40}$$

When $\lambda_T > 0.530$

$$C_v = \frac{1}{0.471 + \lambda_T} \tag{41}$$

The slenderness is

$$\lambda_T = 0.353\frac{h_o}{t}\sqrt{\frac{F_y}{E}} \tag{42}$$

where

$h_o$ = largest distance between the mid-thickness of adjacent walls, in.

### Reliability of the Proposed Method

Because the reliability functions are separated into two groups (yielding, buckling), each group was analyzed separately. Statistical parameters for test-to-predicted strength ratios, $\rho_P$ and $V_P$, as well as the number of specimens, $N$, within each group are listed in Table 3.

From Table 3, $\rho_P = 1.01$ when the proposed equations are used with all specimens. For the 25 specimens controlled by yielding, $\rho_P = 0.932$. When $C_t$ according to Equation 16 is used in lieu of $C$, $\rho_P = 1.03$. However, using $C_t$ is unnecessary because the yield strength bias coefficient offsets the slightly nonconservative nature of using section properties calculated with thin-wall theory.

The anchor point and shape of the buckling curve was adjusted to result in approximately equal reliability for the yielding and buckling limit states. The difference in $\rho_P$ values for yielding and buckling are offset by the differences in $V_P$. Compared to yielding, the buckling limit state has a higher $V_P$; therefore, $\rho_P$ must also be higher to produce similar reliabilities. By comparing the values of $V_P$ for the buckling limit state, it is clear that the proposed design

| Table 3. Statistical Parameters for Test-to-Predicted Strength Ratios Using the Proposed Equations | | | |
|---|---|---|---|
| | **All** | **Yielding** | **Buckling** |
| $N$ | 49 | 25 | 24 |
| $\rho_P$ | 1.01 | 0.932 | 1.10 |
| $V_P$ | 0.183 | 0.118 | 0.189 |
| $N$ = number of specimens | | | |

method is significantly more accurate than the AISC *Specification* equations.

With $\phi = 0.90$, the proposed equations result in $\beta = 2.69$ for the 25 specimens with a predicted failure mode of yielding. With $\beta_T = 2.6$, $\phi = 0.916$. With $\beta_T = 3.0$, $\phi = 0.850$.

With $\phi = 0.90$, the proposed equations result in $\beta = 2.68$ for the 24 specimens with a predicted failure mode of buckling. With $\beta_T = 2.6$, $\phi = 0.917$. With $\beta_T = 3.0$, $\phi = 0.837$.

Figure 8 shows a graph of $T_e/T_y$ versus $\lambda_o$ for the experimental data. The slenderness parameter, $\lambda_o$, is calculated with Equation 43. For the calculation of $\lambda_o$ for the experimental data points, the measured dimensions and material properties were used in lieu of the nominal values. The solid lines plot the proposed design equations, and the AISC *Specification* equations are plotted with dashed lines.

$$\lambda_o = \frac{h_o}{t}\sqrt{\frac{\sigma_y}{E}} \tag{43}$$

## Experimental Failure Modes

The failure mode for each experimental specimen is listed in Table A2 of Appendix A. Compared to the AISC *Specification* equations, the proposed design method results in more accurate predictions of the experimental failure mode. The *Specification* equations provided successful predictions for 38 of 48 specimens for a 79% success rate. The proposed equations provided successful predictions for 44 of 49 specimens for a 90% success rate.

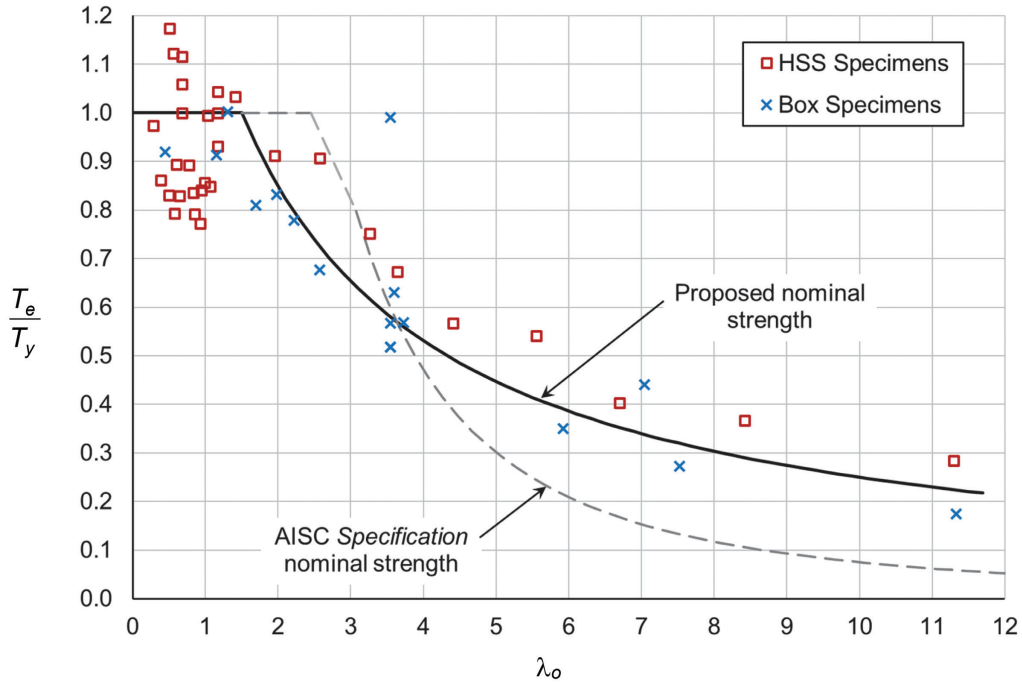


*Fig. 8. Graph of proposed equations with experimental data.*

### Serviceability

For a member subjected to uniform torsion over the length, the twist angle is calculated with Equation 44.

$$\theta = \frac{T_u L}{GJ} \tag{44}$$

where

$G$ = shear modulus of elasticity, 11,200 ksi

$L$ = member length, in.

$T_u$ = uniform torsional moment, kip-in.

$\theta$ = angle of torsional rotation

The twist angle of 20 experimental specimens was reported in the referenced research. These data are shown in Figure 9, where $\theta_{ep}/\theta_c$ is plotted versus $T_{el}/T_p$. $T_{el}$ is the experimental proportional limit torque. $T_p$ is the plastic torsion calculated using Equation 18 with the measured specimen geometry and the measured uniaxial yield stress. $\theta_{ep}$ is the experimental proportional limit rotation. $\theta_c$ is the rotation at torque $T_u = T_{el}$, calculated using Equation 44 with the measured specimen geometry and the measured modulus of elasticity.

As discussed previously in this paper, residual stresses, geometric imperfections, corner stress concentrations, and second-order effects cause yielding at torques lower than $T_y$. This can potentially cause inaccurate serviceability calculations if the serviceability torques are on the nonlinear portion of the torque-rotation curve. To ensure that the serviceability torques are on the linear portion of the torque-rotation curve, the combined effect of residual stresses and geometric imperfections must reduce $T_p$ by no more than 1/1.67 = 0.60. Because the minimum value for $T_{el}/T_p$ is 0.665, this condition is satisfied for all 20 specimens. The mean value of $T_{el}/T_p$ is 0.803.

Figure 9 shows that the experimental rotations generally exceed the rotations calculated with Equation 44. The mean value of $\theta_{ep}/\theta_c$ is 1.22. Because the theoretical equations can significantly underestimate the rotation, this should be considered in the design of critical members where serviceability rotation is the controlling limit state.

## CONCLUSIONS

A review of the available research on the torsional strength of square and rectangular hollow section members revealed 49 experimental tests from 11 projects. Theoretical, experimental, and numerical research identified two strength limit states for members commonly used in buildings: yielding and wall buckling.

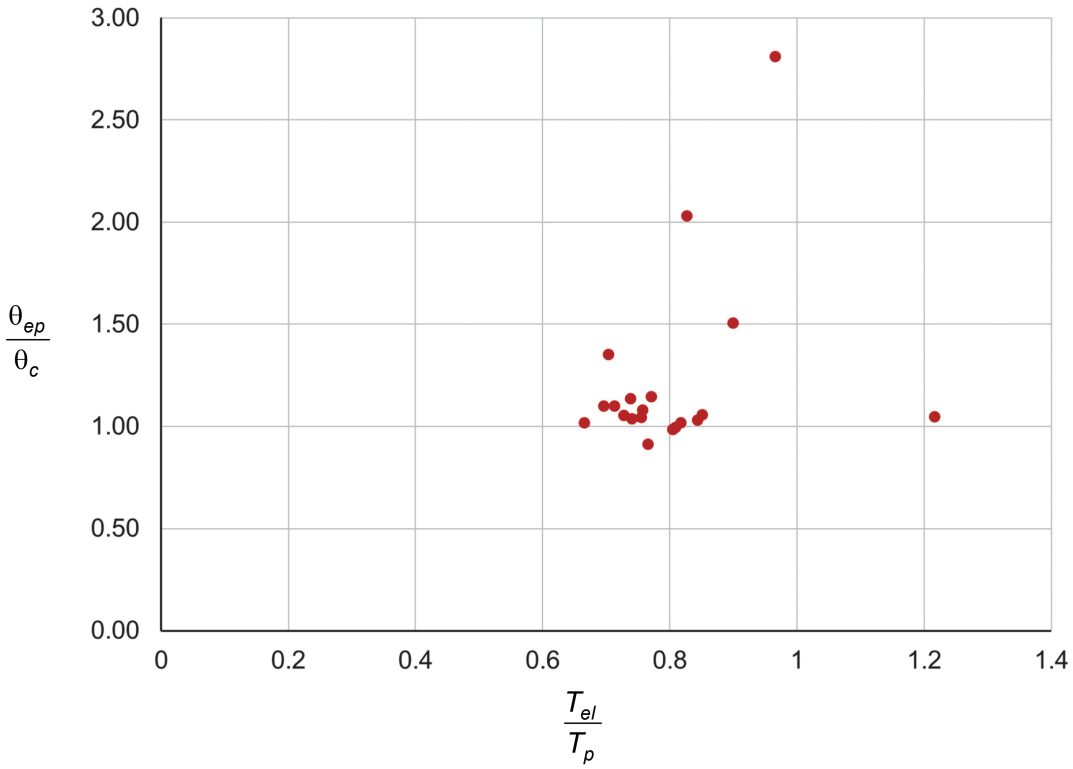


*Fig. 9. Graph of the normalized twist angle versus the normalized yield torsion.*

An evaluation of the AISC *Specification* provisions revealed inconsistent reliability indices that are dependent on the predicted failure mode. The reliability level for the yielding limit state is appropriate. However, for the wall buckling limit state, the reliability index is less than the target reliability index.

Revisions are proposed for the provisions in AISC *Specification* Section H3.1. The improved accuracy of the proposed design method is illustrated in Figure 8, which shows a graph of the normalized strength versus wall slenderness for the AISC *Specification* equations, the proposed equations and the experimental data. In addition to providing a simpler design method and increasing the accuracy, the proposed design equations

- Include provisions for both HSS shapes and box sections.
- Are verified by experimental results.
- Are more successful in predicting the actual failure mode.
- Result in more consistent reliability between the yielding and wall buckling limit states.
- Ensure that the reliability index is greater than the target reliability index for the wall buckling limit state.

The experimental data related to torsional rotation indicated that serviceability torques are low enough to be on the linear portion of the torque-rotation curve. However, the torsional rotations were underpredicted for most of the specimens, with a mean experimental-to-calculated ratio of 1.22. Because the theoretical equations can significantly underestimate the rotation, this should be considered in the design of critical members where serviceability rotation is the controlling limit state.

## SYMBOLS

$A_o$ Area enclosed by the sectional mid-thickness, in.$^2$

$A_w$ Web area, in.$^2$

$B$ Overall width, in.

$C$ Torsional modulus constant, in.$^3$

$C_R$ Correction factor

$C_t$ Torsional modulus constant based on thick-wall theory, in.$^3$

$C_v$ Web shear strength coefficient (Eurocode 3, Part 1-1)

$C_{v1}$ Web shear strength coefficient (AISC *Specification* Section G2.1)

$E$ Modulus of elasticity, ksi

$F_{cr}$ Critical shear stress, ksi

$F_y$ Specified minimum yield stress, ksi

$H$ Overall height, in.

$J$ Torsional inertia constant, in.$^4$

$J_t$ Torsional inertia constant based on thick-wall theory, in.$^4$

$L$ Length, in.

$T_c$ Critical torsional strength

$T_{cm}$ Mean value of the critical torsional strength

$T_p$ Plastic torsion, kip-in.

$T_y$ Yield torsion, kip-in.

$V_E$ Coefficient of variation for modulus of elasticity

$V_G$ Coefficient of variation for the geometric properties

$V_M$ Coefficient of variation for the material properties

$V_P$ Coefficient of variation for the test-to-predicted strength ratios

$V_R$ Coefficient of variation

$V_t$ Coefficient of variation for wall thickness

$V_y$ Coefficient of variation for yield stress

$X_i$ Uncorrelated variables affecting $T_c$

$b_o$ $B - t$

$h$ Flat width of longer side, in.

$h_o$ $H - t$

$k_v$ Buckling coefficient

$p_m$ Mid-thickness perimeter, in.

$r_m$ Mid-thickness corner radius, in.

$r_o$ Outside corner radius, in.

$t$ Design wall thickness, in.

$\Omega_T$ Safety factor for torsion

$\alpha_R$ Separation factor

$\beta$ Reliability index

$\eta$ Shear buckling strength factor

$\lambda$ Slenderness parameter calculated with Equation 38, which uses a buckling width equal to the flat width of longer side, $h$

$\lambda_o$ Slenderness parameter calculated with Equation 43, which uses a buckling width equal to the larger of the two midwall-to-midwall distances for pairs of opposite walls, $h_o$

$\lambda_T$ Slenderness

$\rho_E$ Bias coefficient for modulus of elasticity

$\rho_G$ Bias coefficient for the geometric properties

$\rho_M$ Bias coefficient for the material properties

$\rho_P$ Bias coefficient for the test-to-predicted strength ratios

$\rho_R$ Bias coefficient

$\rho_t$ Bias coefficient for wall thickness

$\rho_y$ Bias coefficient for yield stress

$\sigma_r$ Maximum longitudinal residual stress

$\sigma_y$ Measured uniaxial tension yield stress, ksi

$\tau_{cr}$ Inelastic shear buckling stress, ksi

$\tau_e$ Elastic critical shear stress, ksi

$\tau_p$ Proportional limit shear stress, ksi

$\tau_y$ Shear yield stress, ksi

$\tau_{yr}$ Shear residual stress, ksi

$\nu$ Poisson's ratio

$\phi_T$ Resistance factor for torsion

## REFERENCES


AISC (2023), *Steel Construction Manual*, 16th Ed., American Institute of Steel Construction, Chicago, Ill.

AISC (2022), *Specification for Structural Steel Buildings*, ANSI/AISC 360-22, American Institute of Steel Construction, Chicago, Ill.

Ahlfors, M. (2015), *Distortion and Internal Warping Torsion of a Double Symmetric Hollow Section*, Master's Thesis, Lappeenranta University of Technology, Lappeenranta, Finland.

Al-Ayish, N.A. (2004), "Steel Box Girders under Pure Torsion: A Comparison between Plate and Lattice Box Girders," Master's Thesis, University of Technology, Baghdad.

ASTM (2014), *Standard Specification for Hot-Formed Welded and Seamless Carbon Steel Structural Tubing*, ASTM A501/501M, ASTM International, West Conshohocken, Pa.

ASTM (2015a), *Standard Specification for Cold-Formed Welded Carbon Steel Hollow Structural Sections (HSS)*, ASTM A1085/1085M, ASTM International, West Conshohocken, Pa.

ASTM (2015b), *Standard Specification for Hot-Formed Welded and Seamless High Strength Low Alloy Structural Tubing*, ASTM A618/618M, ASTM International, West Conshohocken, Pa.

ASTM (2021), *Standard Specification for Cold-Formed Welded and Seamless Carbon Steel Structural Tubing in Rounds and Shapes*, ASTM A500/500M, ASTM International, West Conshohocken, Pa.

AWS (2020), *Structural Welding Code—Steel*, AWS D1.1, American Welding Society, Miami, Fla.

Basler, K. (1963), "Strength of Plate Girders in Shear," *Journal of the Structural Division*, American Society of Civil Engineers, October.

Beg, D., Kuhlmann, U., Davaine, L., and Braun, B. (2010), *Design of Plated Structures*, European Convention for Structural Steelwork.

Belingardi, G., Peroni, L., and Scattina, A. (2008), "Experimental Evaluation of the Torsional Behavior of Thin Walled Beams: Elastic and Buckling Situations," *High Performance Structures and Materials IV,* WIT Transactions on the Built Environment, Vol. 97.

Benjamin, J.R. and Cornell, C.A. (1970), *Probability, Statistics and Decision for Civil Engineers*, McGraw-Hill.

Brockenbrough, R.L. (2001), *MTR Survey of Plate Material Used in Structural Fabrication—Part A, Yield-Tensile Properties*, Final Report Submitted to American Institute of Steel Construction, March 1.

CEN (2005), *Eurocode 3—Design of Steel Structures—Part 1-1: General Rules and Rules for Buildings*, European Committee for Standardization, Brussels, Belgium.

CEN (2006), *Eurocode 3—Design of Steel Structures—Part 1-5: Plated Structural Elements*, European Committee for Standardization, Brussels, Belgium.

Chahkand, N.A., Jumat, M.Z., Sulong, N.H.R., Zhao, X.L., and Mohammadizadeh, M.R. (2013), "Experimental and Theoretical Investigation on Torsional Behavior of CFRP Strengthened Square Hollow Steel Section," *Thin-Walled Structures*, Vol. 68.

Chen, D.H. (2016), *Crush Mechanics of Thin-Walled Tubes*, CRC Press.

Chen, S.J. and Chang, S.C. (1993), "Residual Stresses in Welded Jumbo Box Columns," *Journal of Constructional Steel Research*, Vol. 25, pp. 201–209.

Chen, W. (2000), *Plastic Resistance of Thin-Walled Prismatic Tubes under Large Twisting Rotations*, Master's Thesis, Massachusetts Institute of Technology, Boston, Mass.

Chen, W. and Wierzbicki, T. (2000), "Torsional Collapse of Thin-Walled Prismatic Columns," *Thin-Walled Structures*, Vol. 36.

Davison, T.A., and Birkemoe, P. (1983), "Column Behavior of Cold-Formed Hollow Structural Steel Shapes," *Canadian Journal of Civil Engineering*, Vol. 10, No. 1, pp. 125–141.

Derler, C. and Unterweger, H. (2021), "Effects of Warping Torsion on the Buckling Behavior of Slender Box Sections," *CE Papers*, Nos. 2–4.

Devi, S.V., Singh, T.G., and Singh, K.D. (2019), "Cold-Formed Steel Square Hollow Members with Circular Perforations Subjected to Torsion," *Journal of Constructional Steel Research*, Vol. 162.

Dowswell, B. (2021), "Analysis of the Shear Lag Factor for Slotted Rectangular HSS Members," *Engineering Journal*, AISC, Vol. 58, No. 3. pp. 155–164.

ECCS (1976), *Manual on Stability of Steel Structures*, 2nd Ed., European Convention for Constructional Steelwork.

Galambos, T.V. and Ravinda, M.K. (1973), *Tentative Load and Resistance Factor Design Criteria for Steel Buildings*, Research Report No. 18, Department of Civil and Environmental Engineering, Washington University, St. Louis, Mo.

Galambos, T.V. and Ravinda, M.K. (1978), "Properties of Steel for Use in LRFD," *Journal of the Structural Division*, ASCE, Vol. 104, No. ST9, pp. 1459–1468.

Goncalves, R. and Camotim, D. (2013), "Buckling Behavior of Thin-Walled Regular Polygonal Tubes Subjected to Bending or Torsion," *Thin-Walled Structures*, Vol. 73.

Gong, Y. (2008), "Double-Angle Shear Connections with Small Hollow Structural Section Columns," *Journal of Constructional Steel Research*, Vol. 64, No. 5, pp. 539–549.

Han, S.W., Kim, W.T., and Foutch, D.A. (2007), "Tensile Strength Equation for HSS Bracing Members Having Slotted End Connections," *Earthquake Engineering and Structural Dynamics*, Vol. 36, pp. 995–1008.

Hess, P.E., Bruchman, D., Assakkaf, I.A., and Ayyub, B.M. (2002), "Uncertainties in Material Strength, Geometric and Load Variables," *Naval Engineers Journal*, Vol. 114, No. 2, pp. 139–166.

Hovgaard, W. (1937), "Torsion of Rectangular Tubes," *Journal of Applied Mechanics*, ASME, pp. A-131–A-135.

Ingvarsson, L. (1977), *Welding and Cold-Forming Residual Stresses and Their Effect on Buckling of Box Columns of High Strength Steel*, Bulletin No. 130, The Royal Institute of Technology, Stockholm, Sweden.

Key, P.W., Hasan, S.W., and Hancock, G.J. (1988), "Column Behavior of Cold-Formed Hollow Sections," *Journal of Structural Engineering,* ASCE, Vol. 114, No. 2.

Kim, K. and Yoo, C.H. (2008), "Ultimate Strengths of Steel Rectangular Box Beams Subjected to Combined Action of Bending and Torsion," *Engineering Structures*, Vol. 30.

Kitada, T, Nakai, H., and Kunihiro, M. (1989), "Ultimate Strength of Box Stub Columns under Combined Actions of Compression, Bending and Torsion," *Journal of Constructional Steel Research*, Vol. 13.

Konate, M. (2015), *Inelastic Behavior and Strength of Steel Beam-Columns with Applied Torsion*, PhD Dissertation, Old Dominion University, Norfolk, Va.

Li, C., Grondin, G.Y., and Driver, R.G. (2007), *Reliability Analysis of Concentrically Loaded Fillet Welded Joints*, Structural Engineering Report No. 271, University of Alberta, Alberta, Canada.

Liu, J., Sabelli, R., Brockenbrough, R.L., and Fraser, T.P. (2007), "Expected Yield Stress and Tensile Strength Ratios for Determination of Expected Member Capacity in the AISC Seismic Provisions," *Engineering Journal*, AISC, Vol. 44, No. 1, pp. 15–25.

Liu, W., Rasmussen, K.J.R., and Zhang, H. (2017), "Modeling and Probabilistic Study of the Residual Stress of Cold-Formed Hollow Steel Sections," *Engineering Structures*, Vol. 150, pp. 986–995.

Mahendran, M. and Murray, N.W. (1990), "Ultimate Load Behavior of Box-Columns under Combined Loading of Axial Compression and Torsion," *Thin-Walled Structures*, Vol. 9.

Marshall, J. (1970), "Derivation of Torsional Formulas for Multiply Connected Thick-Walled Rectangular Sections," *Journal of Applied Mechanics*, ASME, June.

Marshall, J. (1971), "Torsional Behavior of Structural Rectangular Hollow Sections," *The Structural Engineer*, Vol. 49, No. 8.

Marshall, J. (1972), *Aspects of Torsion of Structural Rectangular Hollow Sections*, PhD Dissertation, University of Strathclyde, Glasgow, Scotland.

Omidvari, A. and Hematiyan, M.R. (2015), "Approximate Closed-Form Formulae for Buckling Analysis of Rectangular Tubes under Torsion," *International Journal of Engineering*, Vol. 28, No. 8.

Osterhof, S.A. and Driver, R.G. (2011), "Performance of the Unified Block Shear Equation for Common Types of Welded Steel Connections," *Engineering Journal*, AISC, Vol. 48, No. 2, pp. 77–92.

Packer, J.A. and Frater, G.S. (2005), "Recommended Effective Throat Sizes for Flare Groove Welds to HSS," *Engineering Journal*, AISC, Vol. 42, No. 1, pp. 31–44.

Peters, R.W. (1954), "Buckling of Long Square Tubes in Combined Compression and Torsion and Comparison with Flat-Plate Buckling Theories," *NACA Technical Note 3184*, National Advisory Committee for Aeronautics.

Rendall, M.A., Hancock, G.J., and Rasmussen, K.J.R. (2018), "Modal Buckling Behavior of Long Polygonal Tubes in Uniform Torsion Using the Generalized cFSM," *Thin-Walled Structures*, Vol. 128, pp. 141–151.

Ridley-Ellis, D.J. (2000), *Rectangular Hollow Sections with Circular Web Openings*, PhD Dissertation, University of Nottingham, Nottingham. England.

Ridley-Ellis, D.J., Owen, J.S., and Davies, G. (2003), "Torsional Behavior of Rectangular Hollow Sections," *Journal of Constructional Steel Research, Vol. 59.*

Schmidt, B.J. and Bartlett, F.M. (2002), "Review of Resistance Factor for Steel: Data Collection," *Canadian Journal of Civil Engineering*, Vol. 29, pp. 98–108.

Seaburg, P.A. and Carter, C.J. (1997), *Torsional Analysis of Structural Steel Members*, Design Guide 9, AISC, Chicago, Ill.

Sharrock, J., Wu, C., and Zhao, X.L. (2015), "CFRP Strengthened Square Hollow Section Subjected to Pure Torsion," *Tubular Structures XV, CRC Press.*

Sherman, D. (1971), "Residual Stresses and Tubular Compression Members," *Journal of the Structural Division*, ASCE, Vol. 97, No. ST3.

Sherman, D.R. (1992), "Tubular Members," Chapter 2.4 in *Constructional Steel Design—An International Guide*, Elsevier.

Smith, F.A., Thomas, F.M., and Smith, J.O. (1970), "Torsion Analysis of Heavy Box Beams in Structures," *Journal of the Structural Division*, American Society of Civil Engineers, March.

Suwan, S., Manuel, L., and Frank, K.H. (2003), *Statistical Analysis of Structural Plate Mechanical Properties*, Final Report Submitted to American Iron and Steel Institute.

Uy, B. (1998), "Local and Post-Local Buckling of Concrete Filled Steel Welded Box Columns," *Journal of Constructional Steel Research*, Vol. 47, pp. 47–72.

White, G.J., Grzebieta, R.H., and Murray, N.W. (1993), "Maximum Strength of Square Thin-Walled Sections Subjected to Combined Loading of Torsion and Bending," *International Journal of Impact Engineering*, Vol. 13, No. 2.

Wittrick, W.H. and Curzon, P.L.V. (1968), "Local Buckling of Long Polygonal Tubes in Combined Compression and Torsion," *International Journal of Mechanical Sciences*, Vol. 10.

Yang, F. and Mahin, S. (2005), "Limiting Net Section Fracture in Slotted Tube Braces," *Steel Tips*, Structural Steel Education Council, April.

Zaifuddin, S.A.M., Chen, D.H., and Ushijima, K. (2017), "Estimation of Maximum Torsional Moment for Multicorner Tubes," *Thin-Walled Structures*, Vol. 112, No. 66–67.

Zhang, X.Z., Liu, S., Zhao, M.S., and Chiew, S.P. (2016), "Comparative Experimental Study of Hot-Formed, Hot-Finished and Cold-Formed Rectangular Hollow Sections," *Case Studies in Structural Engineering*, Vol. 6, pp. 115–129.

Zhao, R.G., Huang, R.F., Khoo, H.A., and Cheng, J.J.R. (2008), "Experimental Study on Rectangular and Square Hollow Structural Section (HSS) Tension Connections," *Canadian Journal of Civil Engineering*, Vol. 35, pp. 1318–1330.

Zhao, X.L., Al-Mahaidi, R., and Kiew, K.P. (1999), "Longitudinal Fillet Welds in Thin-Walled C450 RHS Members," *Journal of Structural Engineering*, ASCE, Vol. 25, No. 8, pp. 821–828.

Zhao, X.L. and Hancock, G.J. (1995), "Longitudinal Fillet Welds in Thin Cold-Formed RHS Members," *Journal of Structural Engineering*, ASCE, Vol. 121, No. 11, pp. 1683–1690.

Ziemian, R.D. (2010), *Guide to Stability Design Criteria for Metal Structures*, 6th Ed., John Wiley & Sons.

Zyczkowski, M. (1991), *Strength of Structural Elements*, Elsevier.

## APPENDIX A

| Table A1. Specimen Details | | | | | |
|---|---|---|---|---|---|
| **Specimen** | ***B* (in.)** | ***H* (in.)** | ***t* (in.)** | ***E* (ksi)** | **$\sigma_y$ (ksi)** |
| Marshall (1972) | | | | | |
| A | 2.00 | 2.00 | 0.193 | 30690 | 44.6 |
| B | 2.50 | 2.50 | 0.193 | 30690 | 44.6 |
| C | 3.00 | 3.00 | 0.193 | 30690 | 62.7 |
| D | 4.00 | 4.00 | 0.252 | 30690 | 44.6 |
| E | 4.00 | 4.00 | 0.161 | 30690 | 44.6 |
| F | 2.00 | 5.00 | 0.252 | 30690 | 44.6 |
| G | 1.50 | 3.00 | 0.161 | 30690 | 44.6 |
| H | 2.00 | 3.00 | 0.130 | 30690 | 44.6 |
| I | 2.00 | 4.00 | 0.130 | 30690 | 44.6 |
| Kitada et al. (1989) | | | | | |
| T-3 | 4.83 | 6.41 | 0.173 | 30023 | 41.9 |
| Mahendran and Murray (1990) | | | | | |
| 1 | 5.94 | 5.94 | 0.0965 | 29000[a] | 31.9 |
| 2 | 5.94 | 5.94 | 0.0748 | 29000[a] | 31.9 |
| 3 | 5.94 | 5.94 | 0.0591 | 29000[a] | 41.3 |
| 4 | 5.94 | 5.94 | 0.0374 | 29000[a] | 41.3 |
| 5 | 5.94 | 5.94 | 0.0295 | 29000[a] | 41.3 |
| 6 | 5.94 | 5.94 | 0.0197 | 29000[a] | 41.3 |
| White et al. (1993) | | | | | |
| 1 | 1.97 | 1.97 | 0.0591 | 29000[a] | 39.0 |
| 2 | 1.97 | 1.97 | 0.0394 | 29000[a] | 36.3 |
| 3 | 1.97 | 1.97 | 0.0299 | 29000[a] | 35.1 |
| 4 | 1.97 | 1.97 | 0.0197 | 29000[a] | 39.2 |
| 5 | 1.97 | 1.97 | 0.0150 | 29000[a] | 85.6 |
| Ridley-Ellis et al. (2003) | | | | | |
| 1 | 3.92 | 7.78 | 0.307 | 28311 | 50.0 |
| 2 | 5.87 | 5.87 | 0.240 | 28311 | 47.8 |
| 3, 4 | 3.94 | 7.83 | 0.312 | 29457 | 55.2 |
| 5 | 5.89 | 5.89 | 0.228 | 28993 | 58.7 |
| I | 1.50 | 1.50 | 0.0563 | 29000[a] | 52.8 |

Table A-1 continues on the next page

| Table A1. Specimen Details (continued) | | | | | |
|---|---|---|---|---|---|
| **Specimen** | ***B* (in.)** | ***H* (in.)** | ***t* (in.)** | ***E* (ksi)** | **$\sigma_y$ (ksi)** |
| Al-Ayish (2004) | | | | | |
| 1 | 5.91 | 15.75 | 0.157 | 29000[a] | 38.0 |
| 2 | 5.91 | 15.75 | 0.157 | 29000[a] | 38.0 |
| 3 | 5.91 | 15.75 | 0.157 | 29000[a] | 38.0 |
| 4 | 5.91 | 15.75 | 0.157 | 29000[a] | 38.0 |
| Belingardi et al. (2008) | | | | | |
| 1 | 1.57 | 1.57 | 0.0394 | 29000[a] | 30.5[b] |
| 2 | 1.57 | 1.57 | 0.0394 | 29000[a] | 30.5[b] |
| 3 | 1.57 | 1.57 | 0.0394 | 29000[a] | 30.5[b] |
| Chahkand et al. (2013) | | | | | |
| 1, 2 | 1.98 | 1.98 | 0.106 | 29008 | 55.4 |
| Sharrock et al. (2015) | | | | | |
| SC-2 | 3.93 | 3.93 | 0.0803 | 29298 | 55.5 |
| SC-3 | 3.96 | 3.96 | 0.115 | 29153 | 62.9 |
| SC-6 | 3.96 | 3.96 | 0.234 | 29153 | 64.4 |
| Konate (2015) | | | | | |
| TR1, TR44 | 1.50 | 1.50 | 0.125 | 29599 | 59.0 |
| Devi et al. (2019) | | | | | |
| P1, P2 | 2.36 | 2.36 | 0.126 | 28355 | 59.8 |
| 1 | 5.91 | 5.91 | 0.0236 | 28355 | 59.8 |
| 2 | 5.91 | 5.91 | 0.0315 | 28355 | 59.8 |
| 3 | 5.91 | 5.91 | 0.0394 | 28355 | 59.8 |
| 4 | 5.91 | 5.91 | 0.0472 | 28355 | 59.8 |
| 5 | 5.91 | 5.91 | 0.0591 | 28355 | 59.8 |
| 6 | 5.91 | 5.91 | 0.0709 | 28355 | 59.8 |
| 7 | 5.91 | 5.91 | 0.0787 | 28355 | 59.8 |
| 8 | 5.91 | 5.91 | 0.0984 | 28355 | 59.8 |
| 9 | 5.91 | 5.91 | 0.315 | 28355 | 59.8 |
| 10 | 5.91 | 5.91 | 0.394 | 28355 | 59.8 |

[a] The modulus of elasticity was not measured for these specimens.
[b] The yield stress was not measured for these specimens.

| Table A2. Experimental Results | | | | | | | | |
|---|---|---|---|---|---|---|---|---|
| | Experimental | | AISC Specification | | | Proposed | | |
| Specimen | $T_e$ (kip-in.) | FM | $T_c$ (kip-in.) | FM | $T_e/T_c$ | $T_c$ (kip-in.) | FM | $T_e/T_c$ |
| Marshall (1972) | | | | | | | | |
| A | 32.5 | Y | 33.3 | Y | 0.974 | 33.3 | Y | 0.974 |
| B | 47.0 | Y | 54.6 | Y | 0.861 | 54.6 | Y | 0.861 |
| C | 90.3 | Y | 114 | Y | 0.793 | 114 | Y | 0.793 |
| D | 157 | Y | 189 | Y | 0.831 | 189 | Y | 0.831 |
| E | 106 | Y | 127 | Y | 0.836 | 127 | Y | 0.836 |
| F | 92.0 | Y | 111 | Y | 0.829 | 111 | Y | 0.829 |
| G | 29.1 | Y | 32.6 | Y | 0.893 | 32.6 | Y | 0.893 |
| H | 33.2 | Y | 37.2 | Y | 0.893 | 37.2 | Y | 0.893 |
| I | 42.6 | Y | 50.2 | Y | 0.848 | 50.2 | Y | 0.848 |
| Kitada et al. (1989) | | | | | | | | |
| T-3 | 254 | Y | 253 | Y | 1.00 | 253 | Y | 1.00 |
| Mahendran and Murray (1990) | | | | | | | | |
| 1 | 105 | B | 126 | Y | 0.831 | 107 | B | 0.981 |
| 2 | 66.9 | B | 94.1 | B | 0.711 | 71.1 | B | 0.941 |
| 3 | 57.7 | B | 55.1 | B | 1.05 | 56.4 | B | 1.02 |
| 4 | 22.7 | B | 13.9 | B | 1.63 | 25.2 | B | 0.902 |
| 5 | 14.0 | B | 6.82 | B | 2.05 | 16.3 | B | 0.858 |
| 6 | 6.00 | B | –[a] | –[a] | –[a] | 7.65 | B | 0.785 |
| White et al. (1993) | | | | | | | | |
| 1 | 9.20 | B | 10.1 | Y | 0.913 | 10.1 | Y | 0.913 |
| 2 | 5.16 | B | 6.38 | Y | 0.809 | 5.89 | B | 0.876 |
| 3 | 3.69 | B | 4.74 | Y | 0.779 | 3.74 | B | 0.986 |
| 4 | 2.21 | B | 2.04 | B | 1.08 | 2.00 | B | 1.10 |
| 5 | 2.58 | B | 0.891 | B | 2.90 | 1.97 | B | 1.31 |
| Ridley-Ellis et al. (2003) | | | | | | | | |
| 1 | 381 | Y | 494 | Y | 0.772 | 494 | Y | 0.772 |
| 2 | 343 | Y | 434 | Y | 0.792 | 434 | Y | 0.792 |
| 3, 4 | 473 | Y | 562 | Y | 0.841 | 562 | Y | 0.841 |
| 5 | 439 | Y | 513 | Y | 0.856 | 513 | Y | 0.856 |
| I | 7.35 | B | 7.39 | Y | 0.994 | 7.39 | Y | 0.994 |

Table A-2 continues on the next page

| Table A2. Experimental Results (continued) | | | | | | | | |
|---|---|---|---|---|---|---|---|---|
| | Experimental | | AISC Specification | | | Proposed | | |
| Specimen | $T_e$ (kip-in.) | FM | $T_c$ (kip-in.) | FM | $T_e/T_c$ | $T_c$ (kip-in.) | FM | $T_e/T_c$ |
| Al-Ayish (2004) | | | | | | | | |
| 1 | 333 | B | 385 | B | 0.865 | 371 | B | 0.898 |
| 2 | 333 | B | 385 | B | 0.865 | 371 | B | 0.898 |
| 3 | 365 | B | 385 | B | 0.947 | 371 | B | 0.984 |
| 4 | 638 | B | 385 | B | 1.66 | 371 | B | 1.72 |
| Belingardi et al. (2008) | | | | | | | | |
| 1 | 3.39 | B | 3.39 | Y | 1.00 | 3.39 | Y | 1.00 |
| 2 | 3.53 | B | 3.39 | Y | 1.04 | 3.39 | Y | 1.04 |
| 3 | 3.16 | B | 3.39 | Y | 0.931 | 3.39 | Y | 0.931 |
| Chahkand et al. (2013) | | | | | | | | |
| 1, 2 | 24.6 | Y | 24.6 | Y | 1.00 | 24.6 | Y | 1.00 |
| Sharrock et al. (2015) | | | | | | | | |
| SC-2 | 72.3 | B | 79.3 | Y | 0.912 | 65.7 | B | 1.10 |
| SC-3 | 133 | B | 129 | Y | 1.03 | 126 | B | 1.05 |
| SC-6 | 278 | Y | 248 | Y | 1.12 | 248 | Y | 1.12 |
| Konate (2015) | | | | | | | | |
| TR1, TR44 | 15.4 | Y | 16.7 | Y | 0.919 | 16.7 | Y | 0.919 |
| Devi et al. (2019) | | | | | | | | |
| 1, 2 | 47.5 | Y | 44.9 | Y | 1.06 | 44.9 | Y | 1.06 |
| 1 | 16.6 | B | 3.46 | B | 4.81 | 13.0 | B | 1.28 |
| 2 | 28.6 | B | 8.27 | B | 3.45 | 22.3 | B | 1.28 |
| 3 | 39.2 | B | 16.3 | B | 2.40 | 33.7 | B | 1.16 |
| 4 | 62.9 | B | 28.4 | B | 2.21 | 46.9 | B | 1.34 |
| 5 | 82.2 | B | 56.1 | B | 1.46 | 69.8 | B | 1.18 |
| 6 | 116 | B | 98.2 | B | 1.19 | 95.9 | B | 1.22 |
| 7 | 144 | B | 136 | B | 1.06 | 115 | B | 1.25 |
| 8 | 216 | B | 227 | B | 0.952 | 167 | B | 1.29 |
| 9 | 783 | Y | 702 | Y | 1.12 | 702 | Y | 1.12 |
| 10 | 997 | Y | 849 | Y | 1.17 | 849 | Y | 1.17 |

$T_c$ = calculated torsional moment, kip-in.
$T_e$ = experimental torsional moment, kip-in.

FM: Failure mode
B: Buckling
Y: Yielding

[a] $h/t = 300$, which exceeds the AISC *Specification* limit of 260.